Plasma-catalytic dry reforming of methane in an atmospheric dielectric barrier discharge: Understanding the synergistic effect at low temperature

X. Tu [1], J.C. Whitehead *

School of Chemistry, The University of Manchester, Oxford Road, M13 9PL, Manchester, UK

ABSTRACT

A coaxial dielectric barrier discharge (DBD) reactor has been developed for plasma-catalytic dry reforming of CH_4 into syngas over different Ni/γ-Al_2O_3 catalysts. Three different packing methods are introduced into the single-stage plasma-catalysis system to investigate the influence of catalysts packed into the plasma area on the physical properties of the DBD and determine consequent synergistic effects in the plasma-catalytic dry reforming reactions. Compared to the fully packed reactor, which strongly changes the discharge mode due to a significant reduction in the discharge volume, partially packing the Ni/γ-Al_2O_3 catalyst either in a radial or axial direction into the discharge gap still shows strong filamentary discharge and significantly enhances the physical and chemical interactions between the plasma and catalyst. Optical emission spectra of the discharge demonstrate the presence of reactive species (CO, CH, C_2, CO_2^+ and N_2^+) in the plasma dry reforming of methane. We also find the presence of the Ni/γ-Al_2O_3 catalyst in the plasma has a weak effect on the gas temperature of the CH_4/CO_2 discharge. The synergistic effect resulting from the integration of the plasma and catalyst is clearly observed when the 10 wt% Ni/γ-Al_2O_3 catalyst in flake form calcined at 300 °C is partially packed in the plasma, showing both the CH_4 conversion (56.4%) and H_2 yield (17.5%) are almost doubled. The synergy of plasma-catalysis also contributes to a significant enhancement in the energy efficiency for greenhouse gas conversion. This synergistic effect from the combination of low temperature plasma and solid catalyst can be attributed to both strong plasma–catalyst interactions and high activity of the Ni/γ-Al_2O_3 catalyst calcined at a low temperature.

1. Introduction

The rapid exhaustion of fossil fuel reserves and the adverse effects of climate change caused by increasing global energy demands have attracted great attention and pose serious threats to humankind. The emergence of new energy technologies is very crucial and essential to reduce the negative effects of climate change and to ensure global energy security based on sustainable and renewable energy sources.

Dry reforming of methane has recently attracted significant interest due to simultaneous utilization and reduction of two abundant and undesirable greenhouse gases, CH_4 and CO_2.

$$CH_4 + CO_2 \rightarrow 2H_2 + 2CO \quad \Delta H^\circ = 247 \, kJ \, mol^{-1} \qquad (1)$$
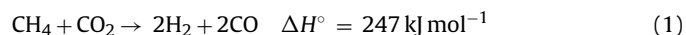
This process generates syngas (H_2 + CO) with a low H_2/CO molar ratio close to 1, which is suitable for the synthesis of value-added oxygenated chemicals and long-chain hydrocarbons. Moreover, this reaction can be carried out with biogas from sources containing large amounts of CO_2 without the pre-separation of CO_2 from the feed. However, dry reforming of methane using conventional catalytic methods still faces two major challenges that limit the use of this process on a commercial scale: firstly, high reaction temperatures (>700 °C) are required to obtain reasonable yields of syngas due to the very endothermic reaction and the strength of the C—H bond in CH_4, incurring a high energy cost; secondly, the formation of severe coke deposition and a subsequent blocking of active metal sites on the catalyst surface, causing rapid deactivation of the catalysts, especially for non-noble metal catalysts [1].

Non-thermal plasma technology provides an attractive alternative to the conventional catalytic route for converting greenhouse gases into syngas and other valuable chemicals because of its non-equilibrium properties, low power requirement and its unique capacity to induce physical and chemical reactions at low temperatures. In non-thermal plasma, the overall gas kinetic temperature remains low, while the electrons are highly energetic with a typical electron temperature of 10,000–100,000 K (1–10 eV), which is sufficient to breakdown inert molecules and produce highly reactive species: free radicals, excited atoms, ions and molecules [2,3]. The

non-equilibrium character of such plasma could overcome thermodynamic barriers in chemical reactions (e.g. dry reforming) and enable thermodynamically unfavorable reactions to occur at atmospheric pressure and low temperatures [4,5]. Several different types of non-thermal plasmas have been investigated for dry reforming of methane including dielectric barrier discharges (DBDs) [6–9], corona discharges [10], glow discharge [11,12] and gliding arcs [13]. The use of a plasma discharge alone has shown that syngas can be generated at low temperatures. However, the selectivities toward the desired products are typically low.

Recently, the combination of non-thermal plasma and heterogeneous catalysis, known as plasma-catalysis for fuel production from hydrocarbon reforming has attracted increasing interest [14,15]. The use of plasma in combination with solid catalysts has the potential to enhance the conversion of feed gases, improve the selectivity toward the desirable products and to reduce the operating temperature of the catalyst which both increases the energy efficiency of the processing and improves the stability of the catalyst by reducing poisoning, coking and sintering [16–19]. Different catalysts have been investigated in single-stage plasma-catalysis systems for dry reforming of methane, including Ni/γ-Al$_2$O$_3$ [20–25], Cu/γ-Al$_2$O$_3$ [25], Ni-Cu/γ-Al$_2$O$_3$ [25], Pd/γ-Al$_2$O$_3$ [26], Ag/γ-Al$_2$O$_3$ [26], La$_2$O$_3$/γ-Al$_2$O$_3$ [27], zeolite [28–30], metal-coated monoliths [31] and ceramic foams [32]. Most of these studies mainly focused on the plasma-catalytic chemical reactions to maximize the process performance, while the interaction mechanisms involved in the combination of plasma with catalyst have received less attention from both physical and chemical perspectives. As we know, the interactions between plasma and catalyst are very complex in a single-stage plasma catalysis system where the catalyst is placed directly in the plasma. Both the chemical and physical properties of the plasma and catalyst can be modified by the presence of each other, which in turn affects the interactions between the plasma and catalyst, consequently changing the performance of the chemical reaction. Previous studies have demonstrated that the interaction of plasma and solid catalyst could generate a synergistic effect, mainly in the plasma-catalysis systems for VOC destruction, which shows the performance of a chemical reaction achieved with plasma-catalysis is better than the sum of those using plasma-alone and conventional catalysis-alone [14,16,17,25]. However, many works have also reported that such a synergistic effect of plasma-catalysis cannot always be observed in a plasma-catalytic reaction, especially for dry reforming reaction using undiluted feed gases [20,21,28,29]. In our previous work, we found that fully packing the Ni/Al$_2$O$_3$ catalyst into the entire discharge region leads to a decrease in conversions of CH$_4$ and CO$_2$ in comparison to plasma dry reforming without catalyst [21]. Packing catalyst pellets into the discharge area is found to shift the discharge mode from microdischarges in the gas to a combination of surface discharge and weak microdischarges, which may partly contribute to the inverse effect of plasma-catalysis. Similar negative effect from the integration of plasma and catalyst has also been reported from other groups [20,28,29], while the reason for this phenomenon has not been discussed and is still not clear. Our recent work has suggested that the synergistic effect of the combination of plasma with catalysis at constant discharge power and low temperatures (without extra heating) for the reforming reaction depends on the balance between the change in discharge behavior induced by the catalyst and the plasma generated activity of the catalyst [30]. The former depends on how the catalysts are packed into the discharge gap and will strongly affect the interactions between plasma and catalyst. However, the detailed understanding of the relationship between the plasma–catalyst interactions and the synergistic effect of plasma-catalysis from both a chemical and physical perspective is still very patchy.

In this work, a coaxial DBD reactor has been developed for the plasma-catalytic dry reforming reaction. The effect of the Ni/γ-Al$_2$O$_3$ catalyst in the discharge gap using different packing approaches on the physical characteristics of the discharge and consequent plasma-catalytic chemical reaction has been investigated. Optical emission spectroscopic diagnostics are employed to understand the reactive radicals in the CH$_4$/CO$_2$ discharge. Catalyst screening using different Ni/γ-Al$_2$O$_3$ catalysts and packing methods is carried out to get a better understanding of the synergistic effect resulting from the combination of non-thermal plasma and solid catalyst.

2. Experimental

2.1. Plasma-catalysis reactor and diagnostic system

Fig. 1 shows a schematic diagram of the experimental setup. The experiment is carried out in a cylindrical DBD reactor, as described in detail in our previous works [21,30,33,34]. The DBD reactor consists of two coaxial quartz tubes, both of which are covered by a stainless steel mesh electrode. The inner electrode is connected to a high voltage output and the outer electrode is grounded via an external capacitor (22 nF). The length of the discharge region is 55 mm with a discharge gap of 3 mm and discharge volume of 11.4 cm^3. CH$_4$ and CO$_2$ are used as feed gases with a total flow rate of 25–100 ml min^{-1} and a mixing ratio of CH$_4$/CO$_2$ = 1:1. The DBD reactor is supplied by an AC high voltage power supply with a peak-to-peak voltage of 24 kV and a variable frequency of 30–40 kHz. The applied voltage is measured by a high voltage probe, while the total current is recorded by a Rogowski-type current monitor (Bergoz CT-E0.25). The voltage on the external capacitor is measured to obtain the charge generated in the discharge. All the electrical signals are sampled by a four-channel digital oscilloscope (Tektronics TDS2014). A LABVIEW control system is used for the online measurement of the discharge power by the area calculation of the Q-U Lissajous figure. An equivalent electrical circuit of the DBD reactor for the calculation of physical parameters (e.g. gas voltage, breakdown voltage) of the discharge can be found in our previous work [21]. Emission spectra of the discharges are recorded by an optical fiber connected to a Princeton Instruments ICCD spectrometer (Model 320 PI, focal length 320 mm) equipped with three gratings (150, 600 and 2400 g mm^{-1}). It offers a resolution of 0.05 nm with a 2400 g mm^{-1} grating.

2.2. Material and analysis

The Ni/γ-Al$_2$O$_3$ catalysts with Ni loading of 10 wt.% are prepared by incipient wetness impregnation using γ-Al$_2$O$_3$ support (AAC Eurovent) and aqueous solution of nickel nitrate (FSA Laboratory). The impregnated catalysts are first dried at 100 °C overnight and then calcined at different temperatures (300, 500 and 800 °C) for 4 h. X-ray diffraction (XRD) patterns of the catalyst samples are recorded by a Philips X'Pert diffractometer using a Cu-K$_\alpha$ radiation at 40 kV and 30 mA in the 2θ range from 20° to 90°. To understand the influence of packing catalyst on the physical and chemical interactions of plasma–catalyst and consequent chemical reaction performance, the Ni/γ-Al$_2$O$_3$ catalyst is packed into the discharge gap using three different packing methods, as illustrated in Fig. 2. In this typical single-stage plasma-catalysis system, the DBD gap consists of two parts: gaseous volume V_g and solid volume V_c. The void fraction of the discharge gap can be defined as:

$$\varepsilon = \frac{V_g}{V_g + V_c} \tag{2}$$

In the packing method A, the supported Ni catalyst pellets are fully packed into the entire discharge gap, which gives a
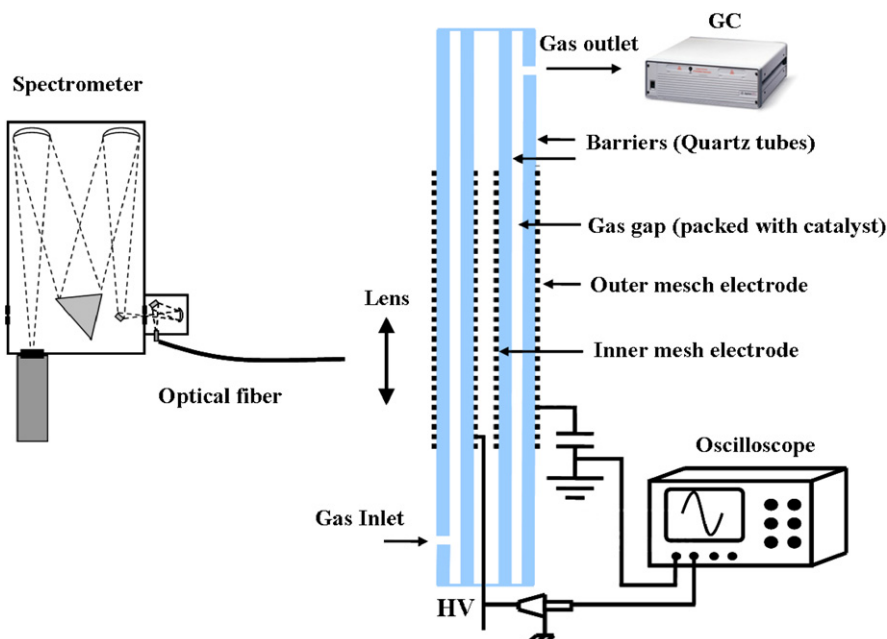
Fig. 1. Schematic diagram of the experiment setup.

small gaseous volume and large volume of the solid catalyst with a very low void fraction. This packing method will generate a typical packed-bed effect [21,33]. In the packing method B, Ni catalyst pellets (1 g) are partially packed into the discharge gap along the radial direction. The catalyst pellets are held by quartz wool and the height of the catalyst bed is about 5 mm. This packing provides a large gas volume and a small volume of the catalyst with a high void fraction (0.90) in the discharge gap. In the packing method C, several pieces of the Ni/γ-Al$_2$O$_3$ catalyst (1 g) in fake form are placed along the bottom of the quartz tube. In this case, quartz wool is only placed outside the discharge gap to hold the catalyst. This partially packing method also provides a large gas volume and a small volume of the catalyst with a high void fraction (0.95) in the discharge gap. The typical gas hourly space velocity (GHSV) and weight hourly space velocity (WHSV) are 263 h^{-1} and 4.03 h^{-1}.

Prior to the plasma-catalytic dry reforming reaction, the Ni/γ-Al$_2$O$_3$ catalyst is reduced in an argon-hydrogen discharge at a discharge power of 50 W (100 ml min^{-1}, 20 vol.% H$_2$) for 30 min in the same DBD reactor.

A trap cooled by solid CO$_2$ is placed at the exit of the plasma reactor in order to condense any liquid products. The feed and
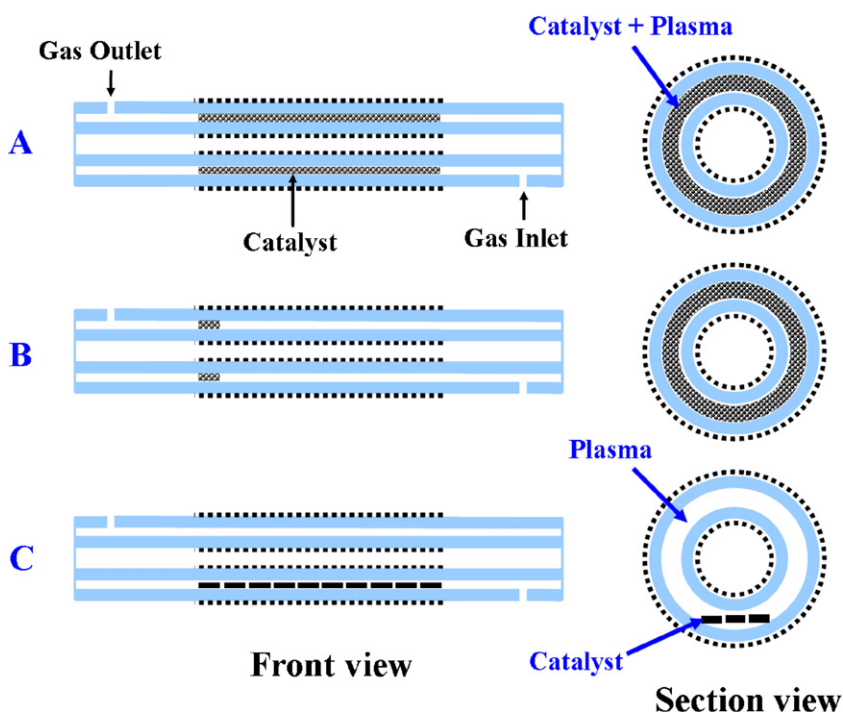

Fig. 2. Different catalyst packing methods in a single-stage plasma-catalysis system.

product gases are analyzed by a two-channel micro gas chromatography (Agilent 3000 A) equipped with two thermal conductivity detections (TCD). The first channel contains a Molecular Sieve 5 A column for the separation of H_2, CO and CH_4, while the second channel is equipped with a Poraplot Q column for the measurement of CO_2 and C_2–C_4 hydrocarbons. The GC is calibrated for a wide range of concentrations for each gaseous component using reference gas mixtures (Agilent Universal Gas Mixture) from Agilent and other calibrated gas mixes.

For the dry reforming reaction, the conversion rates of CH_4 and CO_2 are defined as

$$C_{CH_4}(\%) = \frac{\text{moles of } CH_4 \text{ converted}}{\text{moles of } CH_4 \text{ input}} \times 100 \qquad (3)$$

$$C_{CO_2}(\%) = \frac{\text{moles of } CO_2 \text{ converted}}{\text{moles of } CO_2 \text{ input}} \times 100 \qquad (4)$$

The selectivities, S, and yields, Y, of the products can be calculated

$$S_{H_2}(\%) = \frac{\text{moles of } H_2 \text{ produced}}{2 \times \text{moles of } CH_4 \text{ converted}} \times 100 \qquad (5)$$

$$S_{CO}(\%) = \frac{\text{moles of CO produced}}{\text{moles of } CH_4 \text{ converted} + \text{moles of } CO_2 \text{ converted}} \times 100 \qquad (6)$$

$$S_{C_xH_y}(\%) = \frac{x \times \text{moles of } C_xH_y \text{ produced}}{\text{moles of } CH_4 \text{ converted} + \text{moles of } CO_2 \text{ converted}} \times 100 \qquad (7)$$

$$Y_{H_2}(\%) = \frac{\text{moles of } H_2 \text{ produced}}{2 \times \text{moles of } CH_4 \text{ input}} \qquad (8)$$

$$Y_{CO}(\%) = \frac{\text{moles of CO produced}}{\text{moles of } CH_4 \text{ input} + \text{moles of } CO_2 \text{ input}} \qquad (9)$$

The H_2/CO molar ratio and carbon balance are defined as follows:

$$\frac{H_2}{CO} = \frac{\text{moles of } H_2 \text{ produced}}{\text{moles of CO produced}} \qquad (10)$$

$$B_{Carbon}(\%)$$
$$= \frac{[CH_4]_{out} + [CO_2]_{out} + [CO]_{out} + 2 \times [C_2]_{out} + 3 \times [C_3]_{out}}{[CH_4]_{in} + [CO_2]_{in}} \times 100 \qquad (11)$$

The energy efficiency of a plasma reactor for gas conversion is defined as the number of moles of gas converted per unit of plasma power:

$$E \text{ (mol/J)} = \frac{\text{moles of}(CH_4 \text{ converted} + CO_2 \text{ converted})}{\text{Power}} \qquad (12)$$

3. Results and discussion

3.1. Effect of packing catalyst on physical characteristics of the discharge

Fig. 3 shows the electrical signals of the discharge in the mixing of CH_4 and CO_2 with and without Ni/γ-Al_2O_3 catalyst at a fixed discharge power of 50 W. Using packing method C, we can see that in the presence of the catalyst, the amplitude of several current spikes is larger in comparison to no packing material, showing that the intensity of current pulses has been enhanced. Similar signal profile for the plasma with and without the catalyst suggests that partially
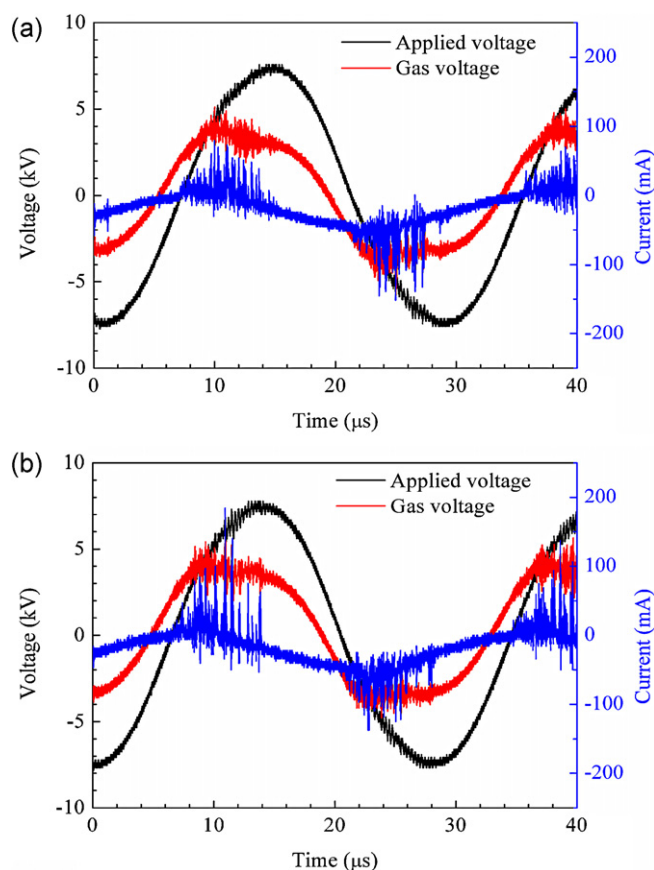

Fig. 3. Electrical signals of the CH_4/CO_2 DBD: (a) without catalyst; (b) partially packed with 10 wt. % Ni/γ-Al_2O_3 catalyst using packing method C (CH_4/CO_2 molar ratio = 1:1).

packing the Ni/γ-Al_2O_3 catalyst into the discharge gap does not significantly change the discharge mode while still exhibits strong filamentary microdischarges due to large volume fraction in the gap. The same characteristics can be found when using packing method B. This behavior is completely different to our previous study in which fully packing the catalyst pellets into the gap (packing method A) significantly decreases the number and amplitude of the current pulses and suppresses the formation of microdischarge due to the significantly reduced discharge volume in the gap ($\varepsilon \ll 1$) [21,30]. This phenomenon indicates that packing method A leads to a significant transition in discharge behavior from a typical filamentary microdischarge to a combination of a spatially limited microdischarge and a predominant surface discharge on the catalyst surface [21,30]. We also found that the presence of fully packed Ni catalyst in plasma leads to a decrease in conversions of CH_4 and CO_2 in comparison with plasma dry reforming reaction without catalyst [21,30]. The negative effect from the combination of plasma and catalysis is related to the weak interactions between the plasma and catalyst induced by the suppression of filamentary discharges. Our recent studies pointed out that the synergistic effect of plasma-catalysis for methane conversion at low temperatures depends on the balance between the change in discharge behavior induced by the catalyst and the activity of the catalyst generated by plasma [30]. In this work, we find that a partial packing method could maintain a strong plasma–catalyst interaction, which is believed to be favorable for the proposed chemical reactions. When the catalyst pellets are fully packed into the gap, the plasma breakdown voltage significantly decreases from 3.3 to 0.75 kV [21]. However, the breakdown voltage of the DBD does not change when the catalyst
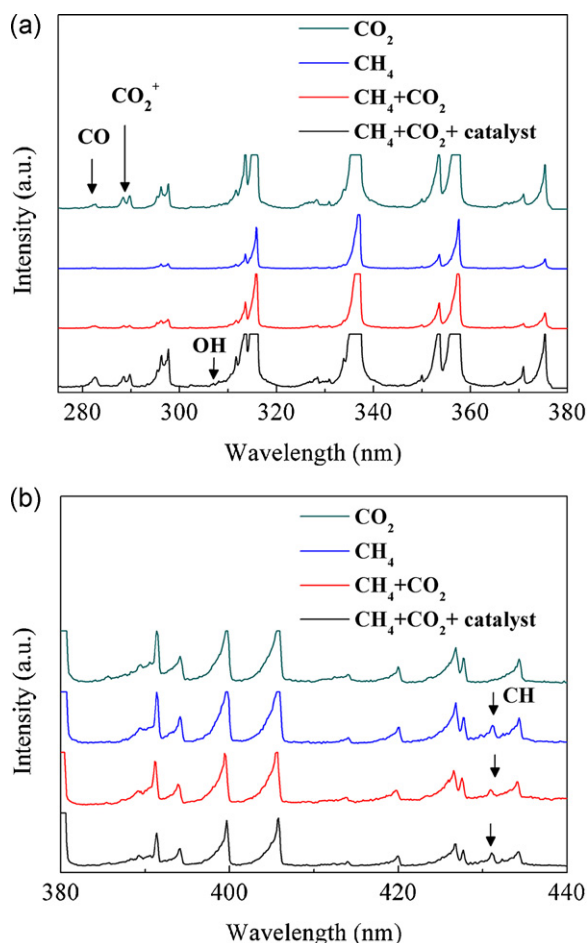
Fig. 4. Optical emission spectra of the discharges with and without catalyst.

Fig. 5. Thermodynamic equilibrium conversion rate of CH_4 and CO_2 as a function of temperature with CH_4/CO_2 molar ratio of 1:1 at 1 atm (without plasma).

is partially packed into the discharge gap either in radial or in axial direction along the quartz tube.

3.2. Emission spectroscopic diagnostics

The spectroscopic technique is performed to measure the emission spectra of the discharge under different conditions, as shown in Fig. 4. All the spectra are clearly dominated by the $N_2(C^3\Pi_u \rightarrow B^3\Pi_g)$ second positive system and $N_2^+(B^2\Sigma_u^+ \rightarrow X^2\Sigma_g^+)$ first negative system between 300 and 450 nm due to an impurity in the gas. At 283 nm, a weak CO band can be found for plasma dry reforming reaction with or without catalyst. It is interesting to note that a double-band of CO_2^+ is also observed at around 290 nm in the discharges containing CO_2

$$CO_2 + e \rightarrow CO_2^+ + e + e \tag{13}$$

We can also find $CH(A^2\Delta \rightarrow X^2\Pi, \Delta v = 0)$ bands at 431 nm in the CH_4 and CH_4/CO_2 discharges. However, $CH(B^2\Sigma^- \rightarrow X^2\Pi, 390\,nm)$ and $CH(C^2\Sigma^+ \rightarrow X^2\Pi, 314\,nm)$ cannot be identified due to the overlap with N_2 or N_2^+ bands. Strong C_2 Swan system at 516 nm and 558 nm can also be clearly seen in the CH_4 DBD. However, these bands are much weaker and partly overlapped with CO bands at 520 nm and 561 nm in the CH_4/CO_2 discharge. Very weak OH $(A^2\Sigma^+ \rightarrow X^2\Pi)$ and NO $(A^2\Sigma^+ \rightarrow X^2\Pi)$ bands can be found in the CH_4/CO_2 discharge with and without the catalyst.

In this work, the rotational temperature of CH is determined by comparing the measured CH (A—X) band to the simulated one using LIFBASE [35]. Due to the high collision and fast rotational relaxation rates in a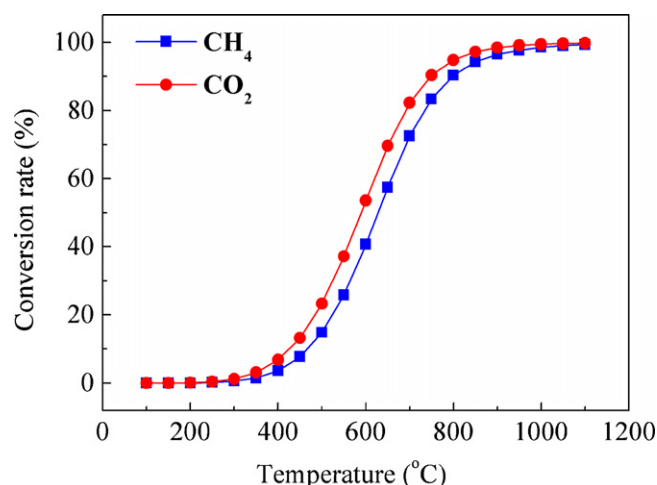tmospheric pressure discharges, it can be assumed that the rotational temperature is very close to the gas temperature. The gas temperature for plasma dry reforming without catalyst is about 270 °C at 50 W. The gas temperature (230 °C) in the discharge partially packed with 1 g Ni/γ-Al_2O_3 catalyst is slightly reduced within the measurement error (± 20 °C).

3.3. Thermodynamic equilibrium calculation

Thermodynamic equilibrium calculation of dry reforming process has been carried out by the method based on the minimization of Gibbs free energy in a closed system. The assumed products include CH_4, CO_2, H_2, CO and H_2O. The total equilibrium concentration of C_2—C_4 hydrocarbons is very low (<0.1%) and can be ignored.

Fig. 5 shows the effect of temperature on the thermodynamic equilibrium conversions of CH_4 and CO_2 (mixing ratio = 1:1) at 1 atm. We can see that the conversion rate of both gases is very low (<1%) below 300 °C. High temperature (>600 °C) is required to get reasonable conversion rate.

3.4. Plasma dry reforming reaction

3.4.1. Plasma dry reforming without catalyst

Plasma dry reforming of CH_4 is carried out using a mixing ratio of $CH_4/CO_2 = 1:1$ and a variable total flow rate of 25–100 ml min^{-1}. H_2 and CO are the major reaction products, while smaller amounts of acetylene, ethylene, ethane, propene and propane are also formed. C_4 hydrocarbons can be seen only at higher discharge power (60 W) or at lower feed gas flow rate (25 ml min^{-1}). Conversions of both CH_4 and CO_2 linearly increase with increasing discharge power as shown in Fig. 6(a) and (b). The conversion rates of CH_4 and CO_2 increase up to 50.4% and 30.5%, respectively, at a discharge power of 60 W and total feed flow of 25 ml min^{-1}. A similar conversion tendency has also been reported in a plasma-catalysis reactor [21]. Previous modeling and experimental studies have shown that increasing plasma power at a constant excitation frequency effectively enhances the electric field, electron density and gas temperature in the discharge [36,37], all of which may contribute in different ways to the improvement in conversion for both gases. In addition, an increase in plasma power produces more active species, such as O and OH, and can also dissociate CH_4 producing more methyl radicals. Increasing discharge power also enhances the production of syngas. We can see that the yield of H_2 and CO increases with the increase in the discharge power, as shown in Fig. 6(c). At the feed flow rate of 50 ml min^{-1}, the maximum yield
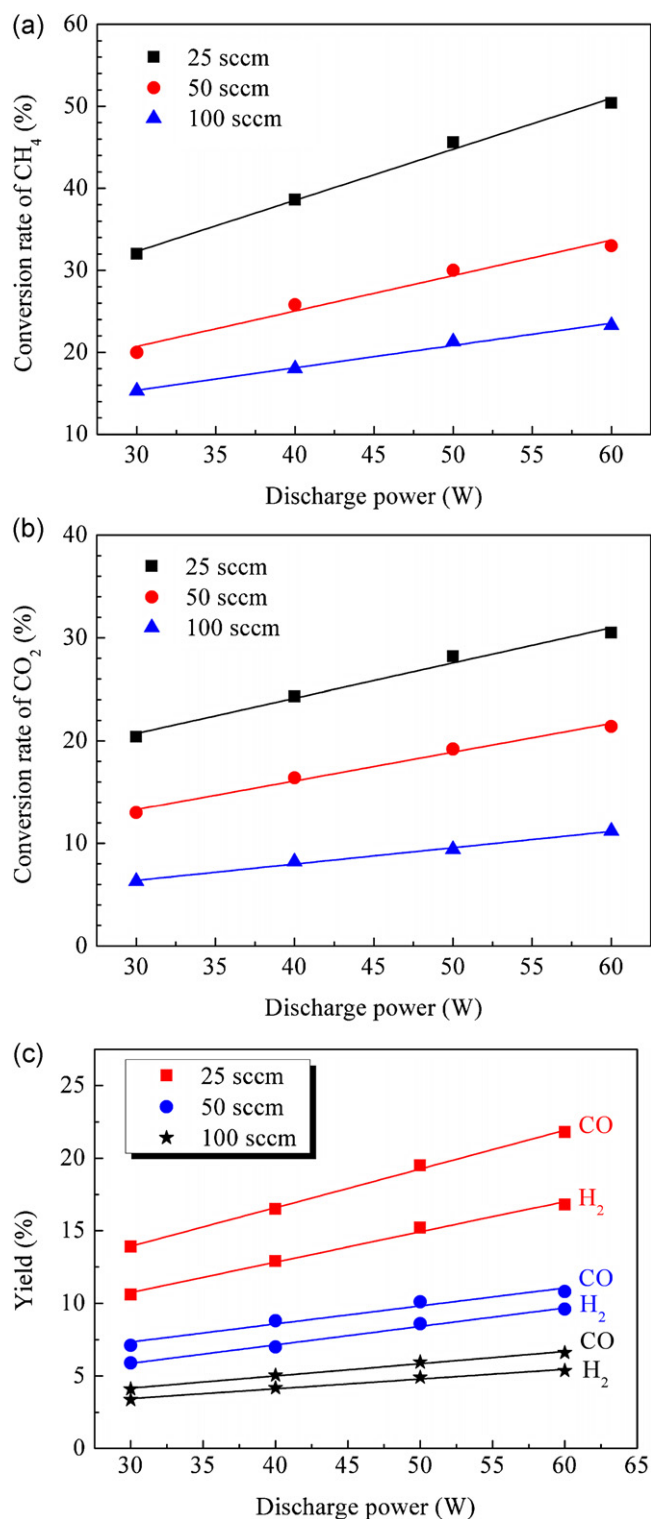
Fig. 6. Plasma-assisted dry reforming of methane without catalyst: (a) conversion rate of CH_4; (b) conversion rate of CO_2; (c) yield of H_2 and CO (CH_4/CO_2 molar ratio = 1:1).

of H_2 and CO is 9.6% and 10.8% respectively at a discharge power of 60 W.

In Fig. 6(a) and (b), we can see that increasing the feed flow rate significantly reduces the conversion of methane and carbon dioxide due to the decrease in the residence time of the feed gas in the discharge area. At a constant discharge power, lower feed flow rate leads to produce syngas with lower H_2/CO ratio and higher
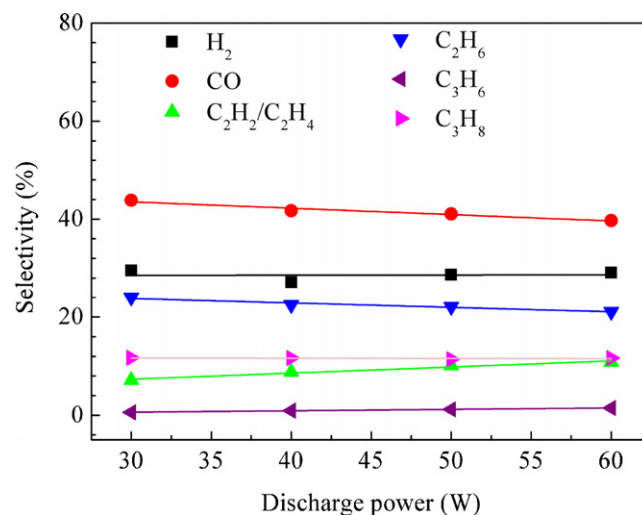

Fig. 7. Selectivities toward syngas and higher hydrocarbons as a function of discharge power in plasma-assisted dry reforming of methane at a feed flow rate of 50 ml min^{-1} (CH_4/CO_2 molar ratio = 1:1).

hydrocarbons (C_4). In this work, the H_2/CO molar ratio decreases from 0.91 to 0.78 when the total feed flow rate changes from 100 ml min^{-1} to 25 ml min^{-1}. In addition, increasing flow rate also significantly decreases the selectivity and yield of syngas. At low feed flow rate of 25 ml min^{-1}, the yield of CO and H_2 reaches its peak of 19.5% and 15.2%, respectively, at 60 W. The results suggest that a lower gas flow rate is beneficial in improving the conversion of CH_4 and CO_2 and producing more syngas.

Fig. 7 presents the selectivity of products as a function of discharge power at the flow rate of 50 ml min^{-1}. The selectivity of CO slightly decreases with a rise in the discharge power, while the selectivity of other products is almost independent of the discharge power between 30 and 60 W. In addition, we find the H_2/CO molar ratio is almost constant with rising discharge power. This effect is consistent with the previous results reported by Song et al. in a non-catalytic DBD reactor [20].

Fig. 8 shows the linear relationship between the conversion of CH_4 and CO_2 for all tested conditions at CH_4/CO_2 molar ratio of 1:1. We find that the conversion rate of CH_4 is always higher than that of CO_2. This behavior has also been reported previously either using non-thermal plasma along or using plasma-catalysis for dry reforming reaction [7,8,25,30]. However, this phenomenon
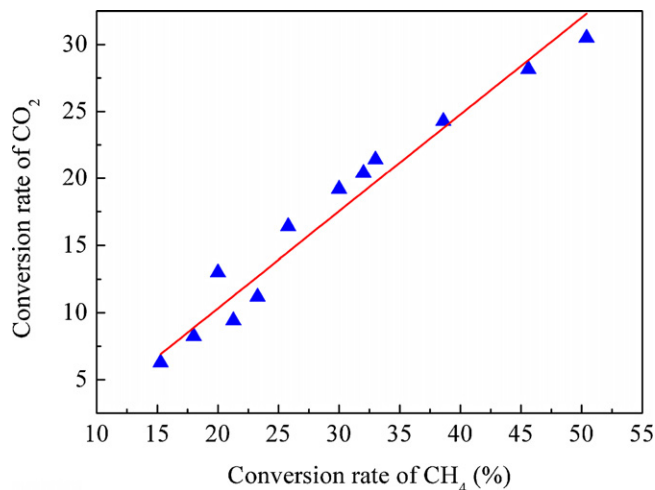

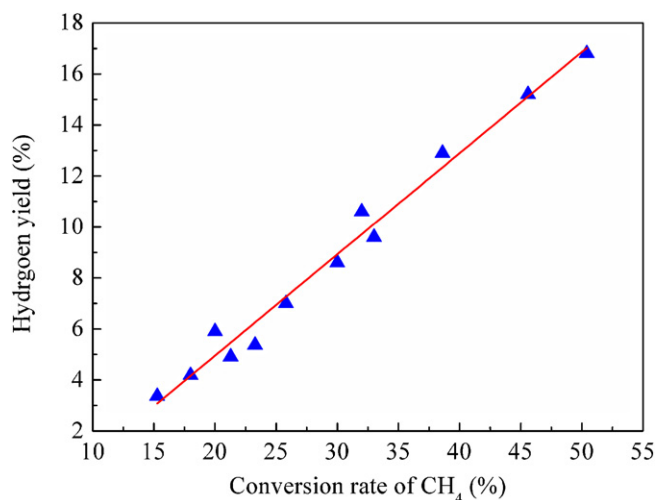**Fig. 8.** CO_2 conversion as a function of CH_4 conversion (CH_4/CO_2 molar ratio = 1:1).

Fig. 9. H_2 yield as a function of CH_4 conversion (CH_4/CO_2 molar ratio = 1:1).

Fig. 10. CO yield as a function of CO_2 conversion (CH_4/CO_2 molar ratio = 1:1).

is different to thermal catalytic dry reforming of CH_4 in which the conversion of CO_2 is generally higher than that of CH_4 due to the simultaneous occurrence of the reverse water gas shift (RWGS) reaction [38,39]. Moreover, thermodynamic equilibrium analysis of this reaction also shows that the conversion rate of CO_2 is higher than that of CH_4 over a wide temperature range (Fig. 5).

From the stoichiometry of the dry reaction reforming of CH_4 (Eq. (1)), equal conversions of CH_4 and CO_2 would be expected. However, we did not observe this under our non-thermal plasma conditions, where CH_4 conversions are always greater than CO_2 conversions. This indicates that more product channels exist for CH_4 conversion such as electron-impact dissociation of CH_4 to generate CH_3, CH_2 and CH (Eq. (14)–(16)), with subsequent radical recombination reactions to form higher hydrocarbons or further electron-impact dissociation of radicals.

$$CH_4 + e \rightarrow CH_3 + H + e \tag{14}$$

$$CH_4 + e \rightarrow CH_2 + H_2 + e \tag{15}$$

$$CH_4 + e \rightarrow CH + H + H_2 + e \tag{16}$$
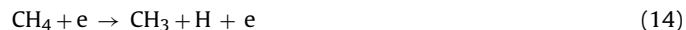
Recent simulation of plasma methane conversion has shown that the reaction (Eq. (14)) is responsible for 79% of the total electron impact dissociation of CH_4, while the reactions (Eq. (15)) and (Eq. (16)) are responsible for 15 and 5%, respectively [40]. The above two reactions (Eq. (14) and (15)) are also the major routes that produce hydrogen, which can be confirmed in Fig. 9, where the yield of hydrogen increases almost linearly with the increase in CH_4 conversion. Direct methane decomposition by electrons could also occur to generate H_2 and solid carbon

$$CH_4 + e \rightarrow C + 2H_2 + e \tag{17}$$

It should be noted the threshold energy for this electron impact dissociate is very high (14 eV) and the average electron energy of DBD is much lower than this value. The electron energy distribution function (EEDF) shows that only a small fraction of the electrons can have such a high energy, which suggests that the formation of carbon deposition can be inhibited if we can control the electron energy distribution in the plasma system. In our experiment, we did not find serious carbon deposition accompanying dry reforming reaction. The carbon balance is between 91 and 96%

Fig. 10 presents the linear relationship between the CO_2 conversion and CO yield, which suggests that the production of CO mainly comes from the dissociation of CO_2. The electron impact dissociation of CO_2 will most likely result in CO in its ground state ($^1\Sigma$) and O atoms in both the ground state (^3P) and the metastable state (^1D).
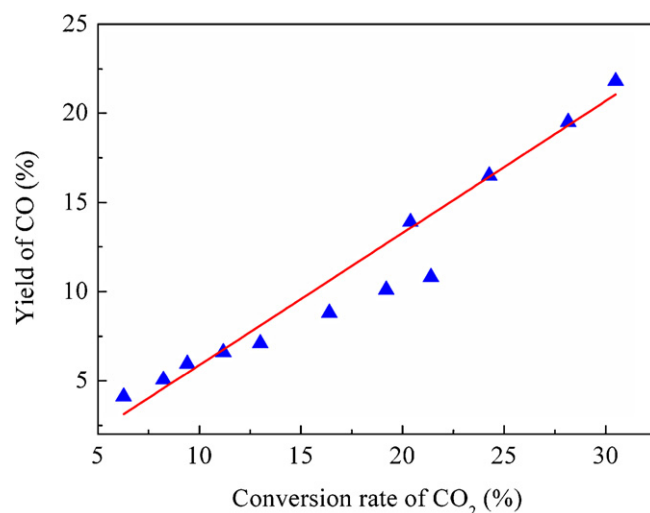
However, since CO bands are observed, same CO is also formed in excited state. Some of the excited atomic oxygen species such as metastable $O(^1D)$ are very reactive and can easily break the C—H bond in CH_4, resulting in a higher conversion of CH_4 and a higher production of methyl radicals.

The low CO_2 conversions can also be a result of the water gas shift (WGS) reaction as shown in equation 18.

$$CO + H_2O \rightarrow CO_2 + H_2 \tag{18}$$

3.4.2. Plasma-catalytic dry reforming reaction

Our recent work has shown that packing supported Ni catalyst into the entire discharge area using packing method A does not exhibit a synergistic effect and leads to a decrease in conversions of CH_4 and CO_2 compared to plasma-assisted dry reforming without a catalyst [21]. We find that how the catalyst is packed in the plasma plays an important role in a single-stage plasma-catalysis system since it significantly determines the physical properties of the discharge and the interactions between the plasma and catalyst, which in turn affects the performance of chemical reactions.

When the 10 wt% Ni/γ-Al$_2$O$_3$ catalyst pellets are partially packed in the discharge gap using packing method B, the conversion rate of CH_4 increases up to 38% compared to the plasma dry reforming with no packing, as presented in Table 1. However, the presence of the Ni catalyst in the discharge has almost no effect on the conversion of CO_2.

It is interesting to note that quartz wool which is generally used to hold catalysts in the reactor also plays an important role in the plasma-catalytic dry reforming reaction. In this study, we can see that the presence of quartz wool in the discharge also leads to an increase in CH_4 conversion (40.2%) and H_2 yield by about 30%. Our recent work has reported that in the presence of

Table 1
Conversion rate, selectivity and yield in plasma-catalytic dry reforming of methane at 50 W (CH_4/CO_2 molar ratio = 1:1; total feed flow rate: 50 ml min^{-1}; 10 wt% Ni/γ-Al$_2$O$_3$ catalyst pellets are partially packed into the gap along the radial direction using packing method B; a: pellet size 0.85–1.7 mm; b: pellet size 0.5–0.85 mm).

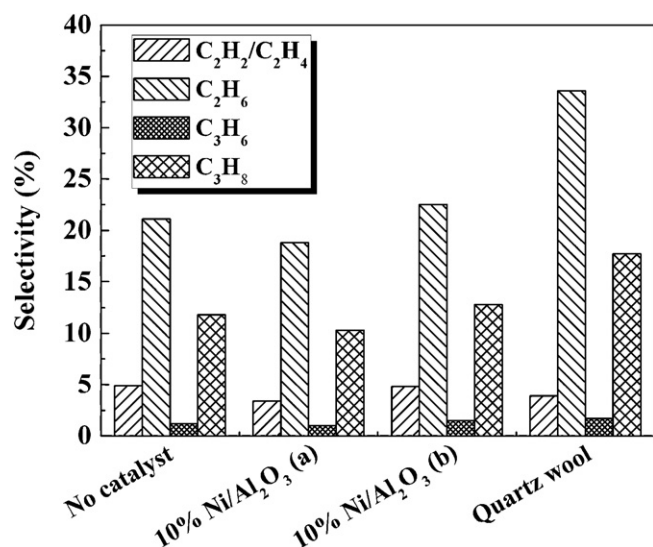|	Conversion (%)		Selectivity (%)		Yield (%)
	CH_4	CO_2	H_2	CO	H_2
No catalyst	30.0	19.2	29.0	44.7	8.7
10% Ni/γ-Al$_2$O$_3$[a]	38.0	21.2	27.6	45.3	10.5
10% Ni/γ-Al$_2$O$_3$[b]	32.0	19.4	32.8	54.9	10.5
Quartz wool	40.2	24.8	30.1	51.4	12.2

Fig. 11. Selectivities toward higher hydrocarbons in plasma-catalytic dry reforming of methane at 50 W (CH_4/CO_2 molar ratio = 1:1; total feed flow rate: 50 ml min^{-1}; 10 wt% Ni/γ-Al$_2$O$_3$ catalyst pellets with different pellet size are partially packed in the gap using packing method B; (a): pellet size 0.85–1.7 mm; (b): pellet size 0.5–0.85 mm).
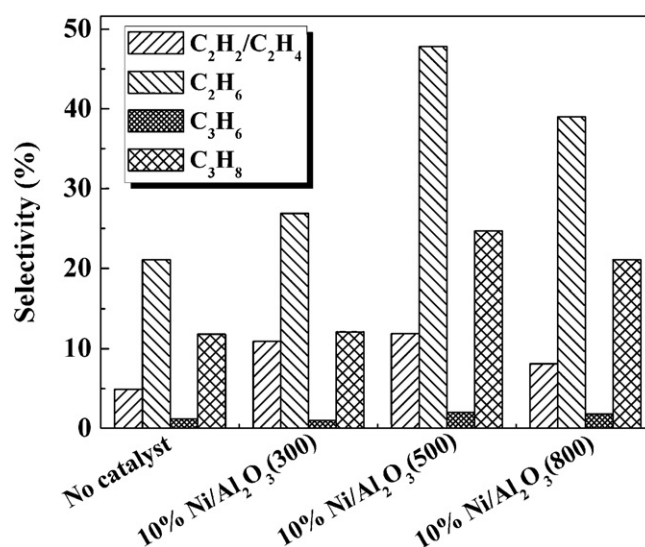

Fig. 12. Selectivities toward higher hydrocarbons in plasma-catalytic dry reforming of methane at 50 W (CH_4/CO_2 molar ratio = 1:1; total feed flow rate: 50 ml min^{-1}; 10 wt% Ni/γ-Al$_2$O$_3$ Ni catalyst in flake form is partially packed in the discharge gap using packing method C; catalysts are calcined at different temperatures from 300 °C to 800 °C).

quartz wool, the amplitude of several current spikes in the plasma is increased in comparison with no packing material, showing that the intensity of current pulses has been enhanced. Quartz wool is a porous material, which leads to a large void fraction of the discharge gap compared with the gap filled with solid pellets (Al$_2$O$_3$ and zeolite 3 A). In addition to intense filamentary discharge, quartz wool also provides a large surface area over which surface discharges can form and propagate. Both effects may contribute the enhancement of the CH$_4$ conversion in the plasma-assisted dry reforming reaction [30]. We have previously reported the use of a microscope-intensified charge coupled device (ICCD) camera to image the observable effects of plasma generation in a CH$_4$/CO$_2$ gas flow on different surfaces in a DBD reactor [41]. Plasma generation was more intense on quartz wool in comparison with no packing material in agreement with the electrical measurements obtained. These findings suggest that the improvement of the reaction performance in the presence of the Ni catalyst pellets (held with quartz wool in the discharge) is likely attributable to the effect of strong plasma-quartz wool interaction rather than the activity of the Ni/γ-Al$_2$O$_3$ catalyst.

As shown in Table 1 and Fig. 11, another interesting phenomenon is that use of a large catalyst pellet size (0.85–1.7 mm) results in a higher methane conversion but gives a lower selectivity toward H$_2$, CO and higher hydrocarbons. A possible explanation of different conversion and selectivity for these two Ni catalysts might be related to the change in physical properties of the discharge due to different pellet size of the catalyst.

Table 2
Conversion rate, selectivity and yield in plasma-catalytic dry reforming of methane at 50 W (CH$_4$/CO$_2$ molar ratio = 1:1; total feed flow rate: 50 ml min^{-1}; 10 wt% Ni/γ-Al$_2$O$_3$ catalyst in flake form is partially packed in the gap using packing method C; catalysts are calcined at different temperatures from 300 °C to 800 °C).

	Conversion (%)		Selectivity (%)		Yield (%)
	CH$_4$	CO$_2$	H$_2$	CO	H$_2$
No catalyst	30.0	19.2	29.0	44.7	8.7
10%Ni/γ-Al$_2$O$_3$ [300]	56.4	30.2	31.0	52.4	17.5
10%Ni/γ-Al$_2$O$_3$ [500]	31.4	14.8	35.4	54.1	11.1
10%Ni/γ-Al$_2$O$_3$ [800]	30.0	15.8	29.2	46.3	8.8

Table 2 shows the results of plasma-catalytic dry reforming of methane over different Ni/γ-Al$_2$O$_3$ catalysts using packing method C. In this method, quartz wool is only placed outside the discharge area in the gas gap to hold the catalyst. Thus, the effect of quartz wool on the reaction performance can be excluded. Compared to the plasma dry reforming reaction in the absence of the catalyst, no positive effect on the conversions of CH$_4$ and CO$_2$ can be observed when using 10 wt.% Ni/γ-Al$_2$O$_3$ catalysts calcined at 500 and 800 °C, respectively. In addition, the presence of the Ni/γ-Al$_2$O$_3$ catalyst significantly increases the selectivity of C$_2$ and C$_3$ hydrocarbons (Fig. 12), but has weak effect on the selectivity of H$_2$ and CO. We also find that the H$_2$ yield decreases with the increase in the calcination temperature for the catalysts. However, it is worth noting that the conversion rate of CH$_4$ and CO$_2$ significantly increases from 30% to 56.4% and from 19.2% to 30.2% when the 10 wt.% Ni/γ-Al$_2$O$_3$ catalyst calcined at 300 °C is placed in the plasma region. The yield of H$_2$ and C$_2$H$_2$/C$_2$H$_4$ is also doubled. Our thermodynamic equilibrium analysis of dry reforming reaction has shown that the conversion rate of both gases is very low (<1%) at low temperatures (e.g. 300 °C), which also means that very low conversions of feed gases can be obtained using thermal catalytic dry reforming reaction at low temperatures (<300 °C). These results clearly show that the performances of the reaction are significantly enhanced with plasma-catalysis, which is much higher than the sum of plasma-alone and catalysis alone, indicating the occurrence of the synergistic effect from the combination of low temperature plasma and supported Ni catalyst calcined at low temperature (300 °C). The carbon content on the catalyst is very low, only 0.6–2.2 wt. % after reaction for 3–4 h.

Previous studies have reported that the Ni-γAl$_2$O$_3$ interactions are strongly affected by the calcination temperature in catalyst preparation process [42]. Higher calcination temperature (e.g. 800 °C) leads to strong interactions between metal (Ni) and support (γ-Al$_2$O$_3$) and results in the formation of NiAl$_2$O$_4$ spinel, which is found to be unfavorable to the reduction of the catalyst, causing a decrease in the catalyst activity for the low temperature reforming reaction. In contrast, lower calcination temperature (e.g. 300 °C) reduces the interactions between Ni and support, and leads to the formation of NiO, which can be reduced at low temperatures. Fig. 13 shows the XRD patterns of the Ni/γ-Al$_2$O$_3$ catalysts calcined at different temperatures. NiO peaks can be clearly seen for the
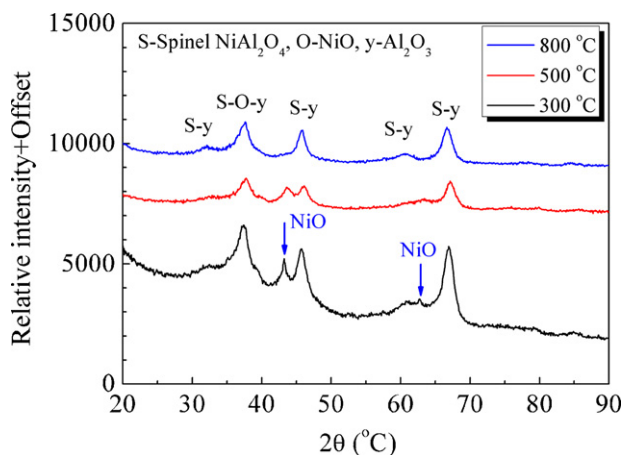
Fig. 13. XRD patterns of the fresh Ni/γ-Al$_2$O$_3$ catalysts calcined at different temperatures.

Ni/γ-Al$_2$O$_3$ catalyst calcined at 300 °C, while these peaks partly or totally disappear for the Ni catalyst using high calcination temperature (e.g. 500 °C and 800 °C). From the XRD spectra, it is difficult to discriminate between NiAl$_2$O$_4$ and γ-Al$_2$O$_3$ as the reflections of these phases overlap. With the increase in calcination temperature, the broaden line at 2θ = 66.6°–66.9° can be observed for the Ni catalyst calcined at 800 °C, suggesting the appearance of NiAl$_2$O$_4$. The blue color of the Ni/γ-Al$_2$O$_3$ catalyst further demonstrates the formation of NiAl$_2$O$_4$ spinel in the Ni catalyst calcined at 800 °C (Fig. 14). In our study, more NiO is generated in the Ni/γ-Al$_2$O$_3$ catalyst when it is calcined at 300 °C. NiO can be easily reduced and activated in the low temperature Ar-H$_2$ plasma, whereas NiAl$_2$O$_4$ in the Ni catalyst cannot be reduced at low temperature. Therefore, the Ni/γ-Al$_2$O$_3$ catalyst calcined at low temperature (300 °C) exhibits higher catalytic activity than the one using high calcination temperature in the dry reforming reaction.

Our recent work has suggested that the synergistic effect from the combination of plasma with catalysis at low temperatures (without extra heating) for the reforming reaction depends on the balance between the change in discharge behavior induced by the catalyst packed into the discharge gap and the plasma generated activity of the catalyst. In this study, we believe that the synergy of plasma-catalysis using packing method C can be attributed to two effects: strong plasma–catalyst interactions due to strong filamentary discharge and the high activity of the Ni/γ-Al$_2$O$_3$ catalyst calcined at low temperature (300 °C). In Table 2, it is also interesting to note that even if the Ni catalysts calcined at high temperature (500 and 800 °C) has a week catalytic activity, the methane conversion can still be kept at a similar level rather than significantly decreasing in the case of fully packing (packing method A) compared to the plasma dry reforming reaction without catalyst. This phenomenon can be ascribed to strong filamentary discharge and consequent strong plasma–catalyst interactions. However, low catalyst activity inhibits the occurrence of the synergy of plasma-catalysis.
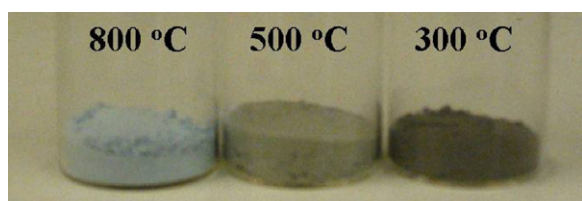

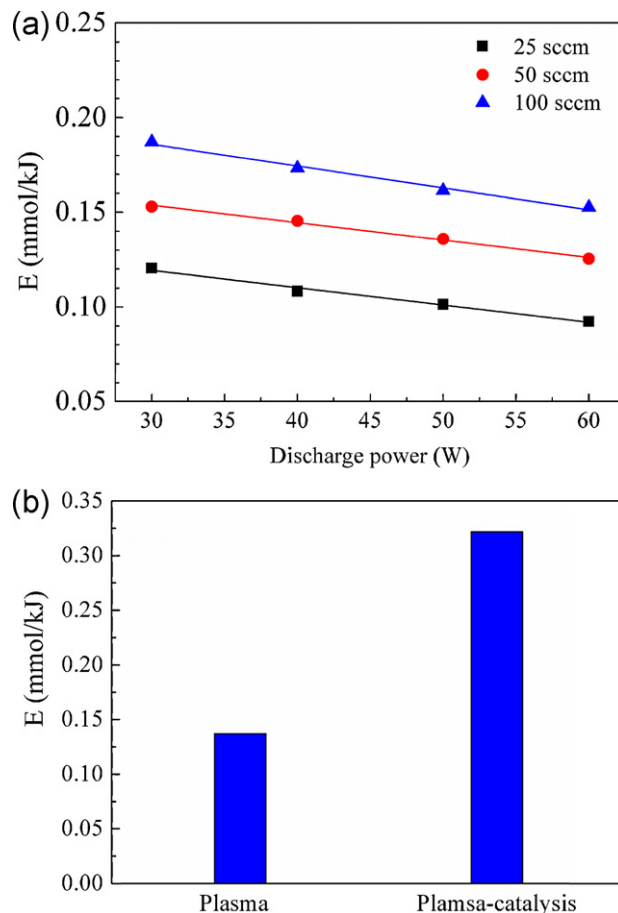**Fig. 14.** Photos of the fresh Ni/γ-Al$_2$O$_3$ catalysts calcined at different temperatures.

Fig. 15. (a) Effect of discharge power and feed flow rate on energy efficiency for CH$_4$ and CO$_2$ conversion (CH$_4$/CO$_2$ molar ratio = 1:1); (b) energy efficiency for CH$_4$ and CO$_2$ conversion using plasma alone and plasma-catalysis at 50 W (CH$_4$/CO$_2$ molar ratio = 1:1, feed flow rate: 50 ml min^{-1}).

3.5. Energy efficiency

Fig. 15(a) shows the effect of discharge power and feed flow rate on the energy efficiency for CH$_4$ and CO$_2$ conversion using plasma alone. We can see that the energy efficiency linearly decreases with the increase in the discharge power even if high conversion of feed gases can be achieved at high discharge power. Similarly, low feed flow rate gives high CH$_4$ and CO$_2$ conversion, but leads to lower energy efficiency for conversion. For plasma dry reforming reaction without catalyst, the maximum conversion efficiency (0.19 mmol/kJ) is achieved at a discharge power of 30 W and a total flow rate of 100 ml min^{-1}. Previous simulation work has shown that the energy efficiency of a plasma chemical reaction could be enhanced by a factor of 4 when using rectangular pulses instead of a sinusoidal voltage [43].

Our results also show that the synergistic effect from the combination of plasma and catalyst significantly enhances the energy efficiency of the plasma dry reforming reaction. Compared to the dry reforming reaction using plasma alone (E = 0.14 mmol/kJ) at a total feed of 50 ml min^{-1}, the conversion efficiency (E = 0.32 mmol/kJ) is significantly enhanced when the 10 wt.% Ni/γ-Al$_2$O$_3$ catalyst calcined at 300 °C is packed in the plasma region, as shown in Fig. 15(b). The conversion efficiency of dry reforming in our experiment is lower than that using thermal plasma and a cold plasma jet [12,44,45] though our results are still comparable to or slightly higher than those using similar DBD systems [23,24,28,31]. Further optimization of the plasma-catalysis system and exploring new catalysts with high activity and stability

is needed to enhance the energy efficiency of the process and make the process economically feasible.

4. Conclusion

In this study, plasma-catalytic dry reforming of CH_4 has been investigated using a DBD reactor combined with different Ni/γ-Al_2O_3 catalysts. Three different packing methods are introduced in this study to get a better understanding of the influence of packing catalysts on the plasma–catalyst interactions and consequent synergistic effect of plasma-catalytic dry reforming reactions.

Compared to the fully packed method, which strongly suppresses the formation of filamentary microdischarges due to a significant reduction in the discharge volume and leads to strongly shifts the discharge mode, partially packing the Ni/γ-Al_2O_3 catalysts either in a radial or axial direction into the discharge area still shows strong filamentary discharge due to the large void fraction in the discharge gap, which significantly enhances the physical and chemical interactions between the plasma and catalyst. However, we find the presence of the Ni catalyst in the plasma has a weak effect on the gas temperature in the CH_4/CO_2 discharge.

The results show that the presence of quartz wool in the DBD reactor effectively improves the conversion of CH_4 in the plasma dry reforming reaction, which can be attributed to the formation of intense filamentary discharge due to the high void fraction of the gap in the presence of quartz wool. When the 10 wt% Ni/γ-Al_2O_3 catalyst in flake form calcined at 300 °C is partially packed in the plasma, the synergy of plasma-catalysis can be clearly observed showing both the CH_4 conversion (56.4%) and H_2 yield (17.5%) are almost doubled. This synergistic effect also contributes to a significant enhancement in the energy efficiency of feed gas conversion. This synergistic effect from the combination of low temperature plasma and solid catalyst can be attributed to both strong plasma–catalyst interactions and high activity of the Ni catalyst calcined at low temperature (300 °C).

Acknowledgments

References

[1] Y.H. Hu, E. Ruckenstein, Advances in Catalysis 48 (2004) 297–345.
[2] A.M. Harling, D.J. Glover, J.C. Whitehead, K. Zhang, Environmental Science and Technology 42 (2008) 4546–4550.
[3] L. Yu, X.D. Li, X. Tu, Y. Wang, S.Y. Lu, J.H. Yan, Journal of Physical Chemistry A 114 (2010) 360–368.
[4] L. Yu, X. Tu, X.D. Li, Y. Wang, Y. Chi, J.H. Yan, Journal of Hazardous Materials 180 (2010) 449–455.
[5] S. Paulussen, B. Verheyde, X. Tu, C. De Bie, T. Martens, D. Petrovic, A.A. Bogaerts, B. Sels, Plasma Sources Science and Technology 19 (2010) 034015.
[6] K.V. Kozlov, P. Michel, H.E. Wagner, Plasmas and Polymers 5 (2000) 129–150.
[7] B.H. Yan, Q. Wang, Y. Jin, Y. Cheng, Plasma Chemistry and Plasma Processing 30 (2010) 257–266.
[8] V.J. Rico, J.L. Hueso, J. Cotrino, A.R. Gonzalez-elipe, Journal of Physical Chemistry A 114 (2010) 4009–4016.
[9] G. Scarduelli, G. Guella, D. Ascenzi, P. Tosi, Plasma Processes and Polymers 8 (2011) 25–31.
[10] M.W. Li, G.H. Xu, Y.L. Tian, L. Chen, H.F. Fu, Journal of Physical Chemistry A 108 (2004) 1687–1693.
[11] A.M. Ghorbanzadeh, R. Lotfalipour, S. Rezaei, International Journal of Hydrogen Energy 34 (2009) 293–298.
[12] D.H. Li, X. Li, M.G. Bai, X.M. Tao, S.Y. Shang, X.Y. Dai, Y.X. Yin, International Journal of Hydrogen Energy 34 (2009) 308–313.
[13] Y.N. Chun, Y.C. Yang, K. Yoshikawa, Catalysis Today 148 (2009) 283–289.
[14] H.L. Chen, H.M. Lee, S.H. Chen, Y. Chao, M.B. Chang, Applied Catalysis B: Environmental 85 (2008) 1–9.
[15] T. Nozaki, W. Fukui, K. Okazaki, Energy and Fuels 22 (2008) 3600–3604.
[16] J. Van Durme, J. Dewulf, C. Leys, H. Van Langenhove, Applied Catalysis B: Environmental 78 (2008) 324–333.
[17] J.C. Whitehead, Pure and Applied Chemistry 82 (2010) 1329–1336.
[18] C.J. Liu, J.Y. Ye, J.J. Jiang, Y.X. Pan, ChemCatChem 3 (2011) 529–541.
[19] C.J. Liu, J.J. Zou, K.L. Yu, D.G. Cheng, Y. Han, J. Zhan, C. Ratanatawanate, B.W.L. Jang, Pure and Applied Chemistry 78 (2006) 1227–1238.
[20] H.K. Song, J.W. Choi, S.H. Yue, H. Lee, B.K. Na, Catalysis Today 89 (2004) 27–33.
[21] X. Tu, H.J. Gallon, M.V. Twigg, P.A. Gorry, J.C. Whitehead, Journal of Physics D: Applied Physics 44 (2011) 274007.
[22] H.L. Long, S.Y. Shang, X.M. Tao, Y.X. Yin, X.Y. Dai, International Journal of Hydrogen Energy 33 (2008) 5510–5515.
[23] M.W. Li, C.P. Liu, Y.L. Tian, G.H. Xu, F.C. Zhang, Y.Q. Wang, Energy and Fuels 20 (2006) 1033–1038.
[24] Q. Wang, B.H. Yan, Y. Jin, Y. Cheng, Energy and Fuels 23 (2009) 4196–4201.
[25] A.J. Zhang, A.M. Zhu, J. Guo, Y. Xu, C. Shi, Chemical Engineering Journal 156 (2009) 601–606.
[26] J. Sentek, K. Krawczyk, M. Mlotek, M. Kalczewska, T. Kroker, T. Kolb, A. Schenk, K.H. Gericke, K. Schmidt-Szałowski, Applied Catalysis B: Environmental 94 (2010) 19–26.
[27] M.H. Pham, V. Goujard, J.M. Tatibouet, C. Batiot-Dupeyrat, Catalysis Today 171 (2011) 67–71.
[28] K. Zhang, B. Eliasson, U. Kogelschatz, Industrial and Engineering Chemistry Research 41 (2002) 1462–1468.
[29] B. Eliasson, C.J. Liu, U. Kogelschatz, Industrial and Engineering Chemistry Research 39 (2000) 1221–1227.
[30] H.J. Gallon, X. Tu, J.C. Whitehead, Plasma Processes and Polymers 9 (2012) 90–97.
[31] V. Goujard, J.M. Tatibouet, C. Batiot-Dupeyrat, Applied Catalysis A-General 353 (2009) 228–235.
[32] M. Kraus, B. Eliasson, U. Kogelschatz, A. Wokaun, Physical Chemistry Chemical Physics 3 (2001) 294–300.
[33] X. Tu, H.J. Gallon, J.C. Whitehead, Journal of Physics D: Applied Physics 44 (2011) 482003.
[34] H.J. Gallon, X. Tu, M.V. Twigg, J.C. Whitehead, Applied Catalysis B: Environmental 106 (2011) 616–620.
[35] J. Luque, D. R. Crosley, SRI Report MP99-009, 1999.
[36] X. Tu, B. Verheyde, S. Corthals, S. Paulussen, B.F. Sels, Physics of Plasmas 18 (2011) 080702.
[37] D. Petrovic, T. Martens, J. van dijk, W.J.M. Brok, A. Bogaerts, Journal of Physics D: Applied Physics 42 (2009) 42.
[38] S. Corthals, J. Van Nederkassel, H. De Winne, Geboers, P. Jacobs, B. Sels, Applied Catalysis B: Environmental 105 (2011) 263–275.
[39] J.K. Xu, W. Zhou, Z.J. Li, J.H. Wang, J.X. Ma, International Journal of Hydrogen Energy 35 (2010) 13013–13020.
[40] C. De Bie, B. Verheyde, T. Marten, J. van Dijk, S. Paulussen, A. Bogaerts, Plasma Processes and Polymers 8 (2011) 1033–1058.
[41] H.J. Gallon, H.H. Kim, X. Tu, J.C. Whitehead, IEEE Transactions on Plasma Science 39 (2011) 2176–2177.
[42] Y.G. Chen, J. Ren, Catalysis Letters 29 (1994) 39–48.
[43] T. Marten, A. Bogaerts, J. van Dijk, Journal of Physics D: Applied Physics 96 (2010) 131503.
[44] X.M. Tao, F.W. Qi, Y.X. Yin, X.Y. Dai, International Journal of Hydrogen Energy 33 (2008) 1262–1265.
[45] X.M. Tao, M.G. Bai, X. Li, H.L. Long, S.Y. Shang, Y.X. Ying, X.Y. Dai, Progress in Energy and Combustion Science 37 (2011) 113–124.